UNIVERSITY OF OKLAHOMA

GRADUATE COLLEGE

NOISE DETECTION AND ESTIMATION IN FREE SPACE OPTICAL COMMUNICATION

A THESIS

SUBMITTED TO THE GRADUATE FACULTY

in partial fulfillment of the requirements for the

Degree of

MASTER OF SCIENCE IN ELECTRICAL AND COMPUTER ENGINEERING

By

NABIL ASFARI
Norman, Oklahoma
2021

NOISE DETECTION AND ESTIMATION IN FREE SPACE OPTICAL COMMUNICATION

A THESIS APPROVED FOR THE
SCHOOL OF ELECTRICAL AND COMPUTER ENGINEERING

BY

Dr. Hazem H. Refai, Chair

Dr. Samuel Cheng

Dr. Choon Yik Tang

DEDICATION

To my parents,

Zeina and Najieb,

&

my beloved siblings,

Faisal, Tarek, Judy and Kareem

ACKNOWLEDGEMENTS

I would like to thank my advisor, *Dr. Hazem Refai*, for his patience, guidance, support, and opportunity to learn. Also, I am tremendously appreciative for giving me the opportunity to undertake and further my studies within his research group at OU-Tulsa in the first place.

I also would like to thank *Dr. Samuel Cheng* and *Dr. Choon Yik Tang* as respected members of my thesis committee. A special acknowledgement of thanks is extended in memory of *Dr. Thordur Runolfsson.*

In addition, I would like to acknowledge the support and motivation from my colleagues and friends during my research, especially Siraj Muhammad and Samuel Chan.

To my extended family at OU, IT department, and staff, I am thankful to you all for everything you have provided me during my time here.

Special thanks to Michelle Farabough for the editing of this thesis.

TABLE OF CONTENTS

LIST OF TABLES

LIST OF FIGURES

ABSTRACT

Free Space Optical Communication (FSOC) has become a popular wireless communications technique for providing and supporting optical high-speed bandwidth data transmission for telecommunication and computer networking. FSOC is expected to supplement traditional Radio Frequency (RF) technologies and successfully aid in removing congestion from the overly crowded RF spectrum, and its optical fiber communications.

FSO system performance is highly dependent on channel conditions, wherein background noise poses a significant problem, even in the absence of weather and/or atmospheric turbulence. Transmitted signals are significantly affected by background noise (e.g., thermal, shot noise, dark currents) primarily on the receiver side, which leads to system performance deterioration. Such effects are often described by Additive White Gaussian Noise (AWGN). This phenomenon affects the communication link and can hinder the accurate detection of information.

The work reported in this thesis investigated the addition of generated AWGN to single FSOC links, as well as the extraction of noise signals at the receiver end via a subtraction method. Test results demonstrated that AWGN can be extracted from an FSOC signal when standard deviation and noise signal mean are estimated using a Gaussian Mixture Model (GMM). Outcomes show there is approximately 80% cross-correlation when compared with an original Pseudorandom Binary Sequence (PRBS) signal.

Chapter 1: INTRODUCTION

1.1 Free Space Optical Communication Technology

The global Free Space Optical Communication (FSOC) market is projected to increase by a compound annual growth rate of ~ 40% from 2018-2023 with sales expanding from USD 0.27 billion to USD 1.45 billion [1]. This escalation can be attributed to an ever-growing need for fast, reliable, secure optical wireless technologies and applications (e.g., area site connection, fiber optic cable network extension to nearby buildings, local loop bypass, backhaul, disaster recovery, last-mile applications, and inter-satellite links, as well as links between spacecraft and satellites, as shown in Figure 1-1 [2]).

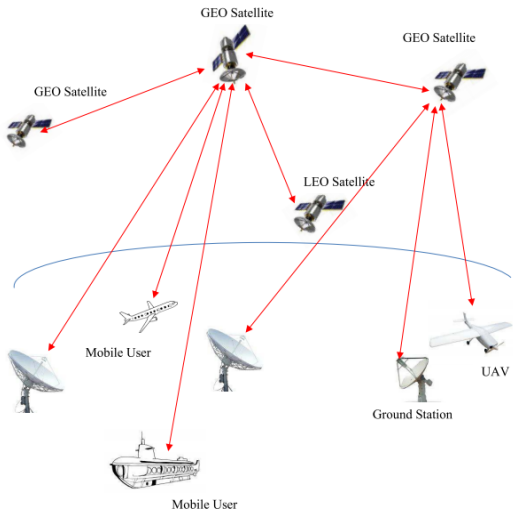

Figure 1-1. Space FSO links.

Radio Frequency (RF) is currently the most commonly used communication technology. Continuing demand for an increase in data and multimedia services has congested the conventionally used RF spectrum. Consequently, there is a need to shift from an RF carrier to an optical one. Furthermore, RF is vulnerable to security threats and susceptible to electromagnetic interference (EMI). Optical wireless communication

(OWC) leverages the optical carrier to transfer data from one point to another through an unguided atmospheric or free space optical channel. OWC is widely recognized as the next frontier for high-speed broadband connection, as it offers high bandwidth, ease of deployment, unlicensed spectrum allocation, reduced power consumption (e.g., ~1/2 of RF), reduced size (e.g., ~1/10 of the RF antenna diameter) and improved channel security [3].

OWC can be classified into two broad categories, namely indoor and outdoor, as shown in Figure 1-2.

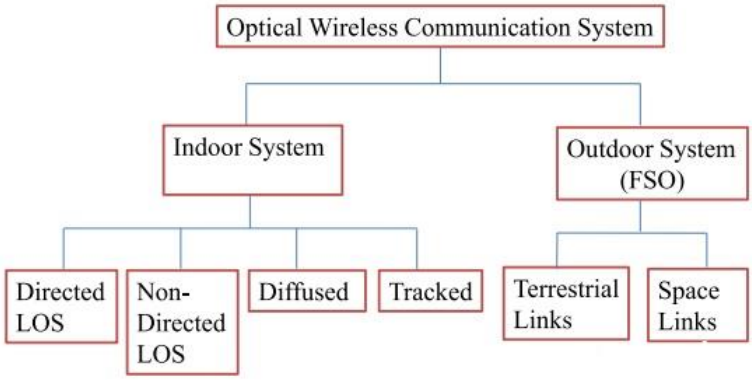

Figure 1-2. Classification of the optical wireless communication system.

Indoor OWC using Infra-Red (IR) or visible light has proven impractical within a building, especially when it is possible to set up a physical wired connection. Outdoor OWC is classified as Free Space Optical Communication (FSOC), which can further be classified into terrestrial and space optical links [2]. Non-directed links (e.g., no requirement for precise alignment between transmitter and receiver) are desirable for applying wireless infrared communication. Links can be categorized as either line-of-sight (LOS) or diffuse. LOS links require an unobstructed path for reliable communication, whereas diffuse links rely on multiple optical paths from surface

reflections. FSOC typically involves directed LOS and point-to-point laser links through the atmosphere from transmitter to receiver. FSOC achieved distances of only a few kilometers has been validated at multi-Gbps data rates [4]. Although FSOC offers higher levels of security and is immune to EMI, it is hindered by limitations. Since an LOS path is required, narrow beam point-to-point FSO links are subject to atmospheric turbulence and obscurations from clouds, rain, fog, snow, and background noise, which degrade performance and risk loss of connectivity. Table 1.1 summarizes the key features of FSOC and RF technologies [5]

Table 1.1. Comparison of FSOC and RF Technologies

Property	FSO	RF
Operating Frequency	THz	GHz
Bandwidth	Unregulated and Unlimited	Regulated and Limited
Data Rate	Medium to High (> Gbps)	Low to Medium (Gbps)
Transmitted Beam Size	Small (2 m)	Large (> 2 m)
Data Density	High	Low
Electromagnetic interference	No	Yes
Line of Sight (LOS)	Yes	No
Multipath Fading	No	Yes
Beam Pattern	High Degree of Control with Lenses	Difficulty to Constrain on Antenna Size
Obstacle Interference	Medium	Low
Services	Communication, Sensing	Communication, Localization
Noise Sources	Sunlight Ambient light	Electrical, Electronic Appliances
Power Consumption	Low	Medium
Mobility	Limited	Good
Latency	Low	High

Assuredly, FSOC will not replace RF communication technology. Rather, the two will co-exist. Hybrid FSO/RF networks are targeted to combine the advantages and circumvent the

disadvantages of each method alone. Although FSO connectivity cannot be available at all times, the aggregated data rate in such networks is clearly greater than RF links used alone.

Available state-of-the-art FSO solutions for space- and air-based networks have been introduced by private companies and government agencies. FSOC is also gaining much interest in space applications [6]. Deep-space Optical Communications will provide a 10X to 100X increase in data returns over present RF space communication (e.g., future advanced instruments, live high definition (HD) video, tele-presence, and human exploration beyond cis-lunar space). Notably, DSOC is considered a radically different operational domain than near-Earth FSOC, primarily due to effects from the vastly increased range between transmitter and receiver. To date, no optical communications link has been closed beyond Earth-Moon distance [7]. Of interest is that the National Aeronautics and Space Administration (NASA) has been pursuing research and development toward deep-space lasercom demonstrations for the past three decades.

1.2 Free Space Optical Communication System Model

FSOC systems are composed of and utilize light that propagates in free space to transmit data for telecommunications and computer networking by leveraging air as its medium. Commonly known as laser communication, FSOC operates in the range of 780-1600 nm wavelength with data transmission of up to 2.5 Gbps [8].

Figure 1-3 illustrates two basic modules requirements, transmitter and receiver—for FSOC system.

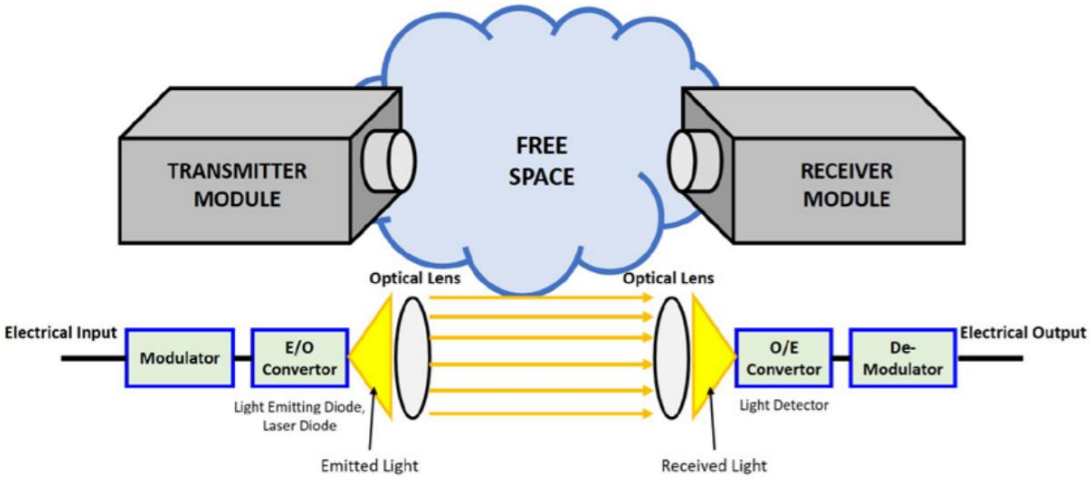

Figure 1-3. Diagram of a simple Free Space Optical Communication system.

The transmitter module consists of a modulator connected to an electrical to-optical convertor (e.g., light-emitting diodes or laser diodes). Through spontaneous emission, the module emits photons with wavelengths corresponding to the energy difference between energy states when an atom drops from a higher to a lower energy level. Photons are focused to optical lenses before transmission into the air medium, primary to shape the light beam propagation and create a collimated ray to minimize light divergence. The receiver module is composed of receiving optical lenses that capture transmitted light. The lenses focus photons to the light detector (e.g., an optical-to-electrical convertor). After passing the de-modulator, the electrical output will then contain the transmitted data.

1.3 Challenges in Free Space Optical Communication

FSO technology uses atmospheric channel as a propagating medium wherein properties are random functions of space and time. This fact makes FSOC a random

phenomenon dependent on weather and geographical location. This section details various challenges to system design in terrestrial and space FSO links.

1.3.1 Line-of-Sight Communication

In the previous section, FSO communication was described as highly dependent on LOS between transmitter and receiver. Additionally, LOS must be maintained throughout the entirety of data transmission. Thus, FSOC network link availability is crucial. Achieving availability might be challenging, as the environment is typically populated with physical obstructions, such as vegetation and buildings. Although, finding a clear LOS for ground-to-ground, ground-to-air and air-to-ground communication might be difficult, finding a clear LOS is definitely possible and advantageous when employing FSOC systems for air-to-air and sea-related communication.

1.3.2 Atmospheric Effects

With air as its medium, FSOC is greatly affected by nature. Atmospheric turbulence can significantly degrade free-space optical link performance. Inhomogeneities in atmospheric temperature and pressure lead to variations of the refractive index along the transmission path. These can deteriorate received image quality and cause fluctuations in both intensity and phase of the received signal, which, in turn, can lead to an increase in link error probability and limit performance. Aerosol scattering effects caused by rain, snow and fog can also degrade FSOC system [9].

1.3.3 Background Noise

The main sources of background noise include a) diffused extended noise from the atmosphere, b) noise from the Sun and other stellar (point) objects and c) scattered light collected by the receiver [10]. Additional sources are detector dark currents, signal shot

noise, and thermal noise. Total noise contribution is the sum of background noise and noise due to other sources. Background noise is a significant problem for FSOC, even when there are no weather or atmospheric turbulences. Contributions of background noise, thermal noise and dark current noise are modeled and described as AWGN [11], which describes background noise attributes: 'additive' to the received desired signal; 'white' flat spectral density over a wide range of frequencies; and follows 'Gaussian' distribution.

1.4 Modulation Schemes in Optical Wireless Communication

In optical wireless systems, the intensity of an optical source is modulated to transmit signals. For digital data transmission, there are no practical alternatives to digital modulation since the process provides source coding (e.g., data compression), channel coding 40 (e.g., error detection/correction), and easy multiplexing of multiple information streams [12]. Digital data transmission can be accomplished on a bit-by-bit basis (e.g., binary encoding) or on a bit-word basis (i.e., block encoding).

1.4.1 On-Off Keying

The simplest type of binary modulation scheme is one-off keying (OOK). In an active high OOK encoding, a 'one' is coded as a pulse, while a 'zero' is coded as 'no' pulse or an 'off' field. To restrict the complexity of the modulator, pulse shape is rectangular. Bit rate is denoted as $R_b = 1/T_b$, where T_b is the bit duration and is directly related to the rate at which the source can be switched on and off. Normalized transmit pulse shape for OOK is given by

$$p(t) = \begin{cases} 1, & for\ t \in [0, T_b) \\ 0, & elsewhere \end{cases} \qquad \text{Eq (1)}$$

Given that channel impulse response $h_c(t)$ is a delta function and the received signal is corrupted by only AWGN, then the resulting channel is deemed an AWGN channel. Consider a binary digital communications system where signals $p_1(t)$ and $p_2(t)$ represent data bits '1'and '0', respectively. The received signal r(t) over an AWGN channel can be expressed as,

$$r(t) = \begin{cases} p_1(t) + n(t), & if\ transmitted\ bit\ is\ '1', \\ p_2(t) + n(t), & if\ tramissted\ bit\ is\ '0' \end{cases} \quad \text{Eq (2)}$$

OOK modulation was adopted as the modulation scheme in the study reported in this thesis. OOK is a binary level modulation format widely used in FSOC due to its simplicity and high-power efficiency [13].

1.5 Thesis Objective

The contribution of the work presented in this thesis is discovering answers to the following research questions through data collection, preprocessing, analysis, subtracting, and applying a gaussian mixture model (GMM).

1. Can we emulate the effects of a background noise signal that affects and limits the performance of an FSOC signal?

2. Can we extract and separate the known additive noise from a generated FSOC signal, using the subtraction method?

3. If the parameters sigma (σ) and mu (μ) for additive noise signals are unknown, can we estimate parameters, and then extract and separate the noise from the combined, noisy signal?

1.6 Thesis Outline

The thesis is organized as follows.

- Chapter 2 presents background information and a literature review for FSOC systems, as well as a summary of the accompanying challenges of background noise and atmospheric turbulence.
- Chapter 3 presents the experimental accumulation and detection of additive noise in FSOC signals. Experimental setup, data collection, analysis, and results are also described.
- Chapter 4 introduces the GMM, providing a description, the motivation behind utilizing the model, and the way in which the model is implemented to estimate parameters for additive noise in an FSOC signal.
- Chapter 5 summarizes the thesis' conclusions, proposes possible future work and emerging developments.

Chapter 2: BACKGROUND AND LITERATURE REVIEW

FSOC systems have garnered much interest because of the technology's ability to meet the growing demand of high-data-rate connection and to be rapidly deployed [2]. Some terrestrial FSO products provide data rates on the order of Gbps, which is much greater those provided by digital subscriber lines or coaxial cables [4]. Additionally, the installation of an FSO system requires only a few days, making it flexible and effective for deployment. Recently, FSOC system applications have advanced to include high data-rate hybrid networks (i.e., RF/FSO hybrid communication systems) for high speed connection, ultra-low latency networks for stock market trading [5], and quickly deployed networks for communication recovery).

FSOC systems can be categorized into two types: intensity modulation with direct detection (IM/DD) and coherent. In an IM/DD system, the lens system and photodetector operate to detect the instantaneous power in the collected field when it arrives at the receiver. In coherent systems, the collected field is optically mixed with a local generated field through a front-end mirror before reaching the photodetector.

OOK modulation is widely used for IM/DD FSOC systems, since those with higher order modulation are complex to implement [14, 15]. In [16], the authors described several communication techniques to mitigate turbulence-induced intensity fluctuations for an IM/DD OOK system.

The building sway problem for an FSO system with OOK modulation was studied in [17]. In [18], the authors presented error rate performance bounds for an OOK FSOC system over K fading channels. In [15], a multiple-input multiple-output (MIMO) FSO link over K turbulence channels was studied, wherein IM/DD with OOK modulation was

assumed. In [19], the authors analyzed the OOK FSOC system performance with Hoyt distributed misalignments. In [20], the authors conducted an experimental evaluation of error performance for IM/DD FSOC links with various modulation schemes, including OOK, pulse position modulation (PPM) and binary phase-shift keying (BPSK). In coherent FSO systems, the provision of phase information allows a variety of digital modulation formats when compared to irradiance modulation with direct detection IM/DD. In such systems, the signal can be amplitude-, frequency- or phase-modulated on the optical carrier. Received signals can be made shot-noise-limited through the use of a local oscillator.

The main challenge in FSOC system design is that the deleterious effects in the atmospherical channel can severely degrade performance. Atmospheric attenuation can sometimes cause FSOC system outage, which also considerably limits its link range. Another adverse effect in atmospheric channel is scintillation caused by thermally induced changes in the refraction index of air along the beam transmit path. As a result, the received irradiance at receiver will randomly fluctuate. Such fluctuation can dramatically degrade FSOC system performance [20, 21]. In addition to scintillation effects, pointing and alignment can also affect FSOC system performance. Due to building sway and beam wander effects, accurate pointing cannot be easily achieved. In terrestrial FSOC systems, transceivers are often positioned at the top of tall buildings to obtain LOS. In satellite-to-ground and intersatellite communications, transmitter and receiver have high relative velocity, and there is mechanical noise due to satellite-based motion and gimbal friction [22]. Thus, it is difficult to realize perfect tracking; jitter and boresight can also arise as residual pointing error. In [17], the author proposed a

mathematical model to minimize transmitter power and the beam divergence angle in an urban optical wireless communication system with pointing errors caused by building sway. In [23], a maximum-likelihood estimator was developed to approximate the boresight and jitter component of the pointing error; a point detector and nonzero boresight component are assumed. In a follow-up work [24], the same authors further considered the effects of atmospheric turbulence for the lognormal and Gamma-Gamma fading channels, and they adopted a wave optics-based approach to evaluate channel capacity.

An experimental demonstration of FSO multi-user communication is reported in [25]. The authors characterized an optical link by three independent users and a dual-path fiber bundle receiver. In their previous work, diverse O-MAC techniques (e.g., independent component analysis (ICA), non-orthogonal multiple access, signal subtraction), proved to support high-data rate multi-user communication successfully and accurately. However, previous techniques were tested separately with various experimental setups.

The authors overcame the limitations of each method, and, in order to consider potential Channel State Information (CSI) availability at the receiver side, they proposed and experimentally evaluated combinations of the various O-MAC techniques (i.e., ICA and NOMA, ICA and subtraction, NOMA on one received mixed signal, and NOMA on both the received mixed signals). NOMA on both received signals proved to demodulate the signals with the greatest accuracy, although CSI at both receivers was required. ICA-and-NOMA combination and ICA-and-subtraction combination reconstructed transmitted signals with a mean cross-correlation greater than 0.9 between the three users. Notably,

no prior work has been reported on the subtraction of known AWGN for reconstructing the original transmitted signal nor on the addition for estimating additive noise parameters, when limited CSI is available at the receiver side.

Chapter 3: METHODOLOGY

3.1 Experimental Setup

The FSO experimental setup used for research reported in this thesis is shown in Figure 3-1. Figure 3-1(a) depicts a flow diagram, and 3-2(b) depicts the hardware device configuration. Perfect alignment was assumed between transmitter and receiver. Furthermore, perfect time synchronization of the system and absence of intersymbol interference was also assumed. The setup included one user based on an intensity modulation—namely OOK—with direct detection scheme and an additive noise signal.

In the Figure 3-1(a) block diagram, the black solid lines connecting the blocks represent electrical links; the red solid lines represent the optical fiber connections; and the blue dashed lines represent the free space optical links. Additive noise was generated using SIGLENT'S SDG6032X function generator and its noise waveform function, which generates white gaussian noise, driven using ThorLabs MX10B high-speed (e.g., 12.5 Gbps) Digital Reference Optical Transmitter at a 1550 nm optical wavelength, with an integrated tunable C-band laser source.

User 1 consisted of a 1310 nm optical module transceiver (SFP) driven via Hitech Global SMA-to-SFP board by a PRBS, featuring $2^5 - 1$ bits length, 300 Mbps data-rate, 1.000 Vpp Amplitude and 2.8ns Rise/Fall. The PRBS signal was generated with one independent, dual-channel pulse/arbitrary waveform generator, namely SIGLENT's SDG6032X.

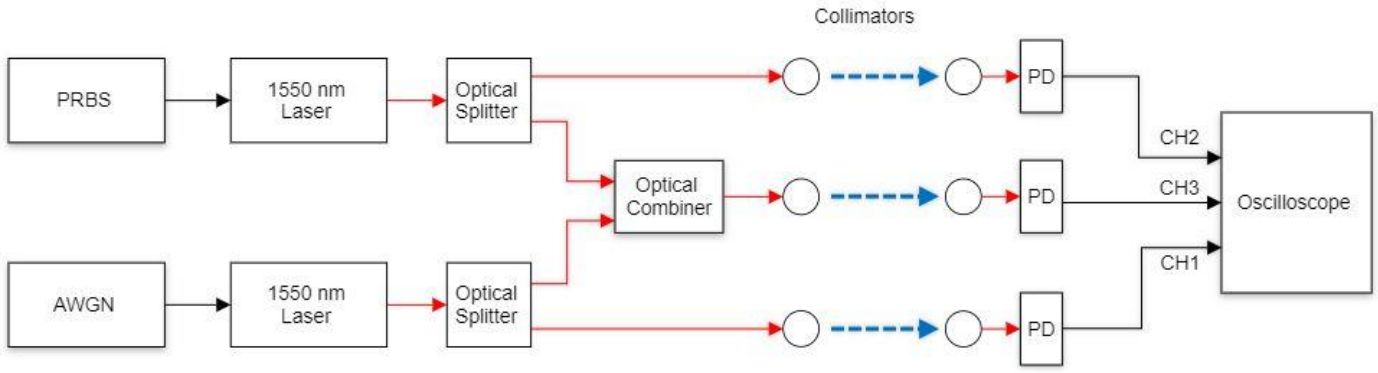

(a) Depiction.

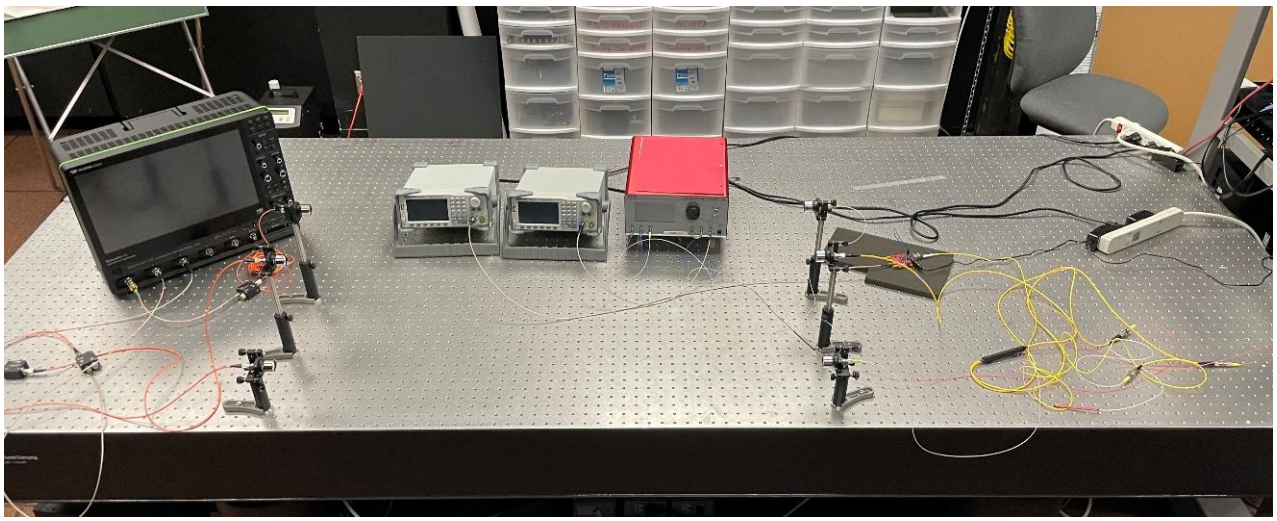

(b) Picture.

Figure 3-1. Experimental setup.

PRBS and AWGN signals were split into two outputs with equal power, using ThorLabs' 10202A-50-FC 50:50 Splitter (See Figure 3-2) to facilitate oscilloscope data collection. PRBS and AWGN signals were combined using ThorLabs' WD1350F - 1310 nm / 1550 nm Wavelength Division Multiplexer, (See Figure 3-3), which is designed to

combine the two 1310 nm and 1550 nm signals with a ∓15.0 nm bandwidth around the center wavelength of each channel wavelength.

Figure 3-2. ThorLabs' 10202A-50-FC 50:50 Splitter.

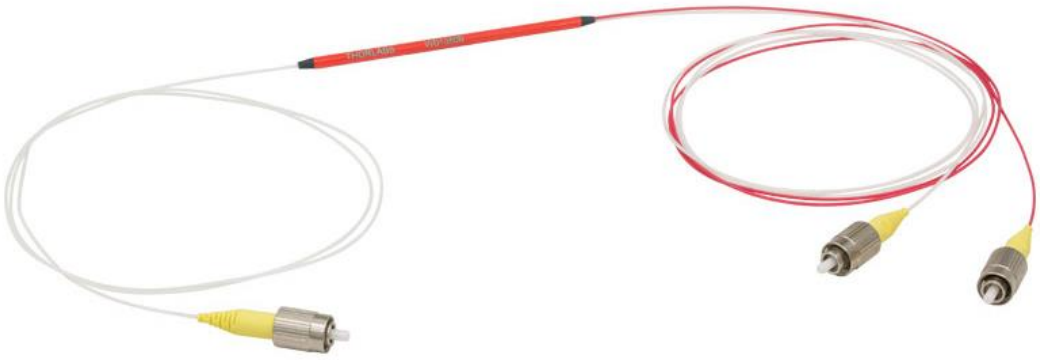

Figure 3-3. ThorLabs' WD1350F – 1310/1550 nm Wavelength Division Multiplexer.

Two collimators with 37.17 mm focal length (i.e., 1550 nm wavelength dependent) were used for transmission and reception of the signals (See Figure 3-4[a]). Additionally, one collimator with 36.90 mm focal length (i.e., 1310 nm wavelength dependent) was also utilized for transmission and reception of these optical signals (See Figure 3-4[b]).

(a) 1550 nm wavelength dependent.

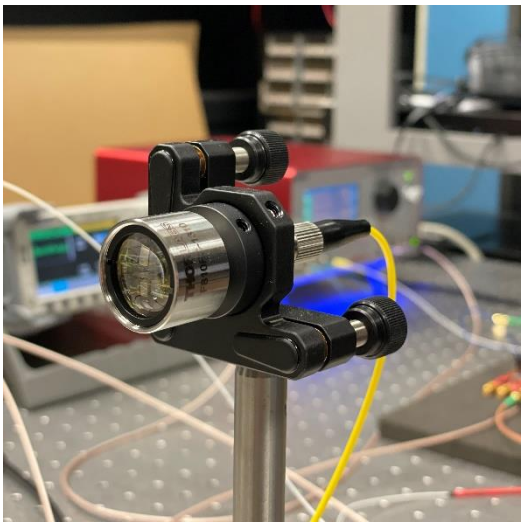

(b) 1310 nm wavelength dependent.

Figure 3-4. Transmission and reception collimators.

3.2 Data Collection

The combined (PRBS + AWGN), PRBS, and AWGN signals were propagated through free space for 1.1-m independently, and then collected by three 5 GHz InGaAs photodetectors, namely ThorLabs DET08CFC, (See Figure 3-5), which were used for

optical-to-electrical conversion. Although three wavelengths were employed at the transmitting side, no wavelength selective filter was implemented at the receiving side. Photodetector outputs were then connected to a WavePro 254HD-MS Oscilloscope with a 20 GSample/s sampling rate for data collection and visualization, including the combined (PRBS + AWGN), PRBS, and AWGN signals, simultaneously.

Figure 3-5. ThorLabs' DET08CFC 5 GHz InGaAs photodetector.

3.3 Data Analysis

After the optical-to-electrical conversion, 100,000 samples were collected for each of the three optical signals examined in this research. Acquired data was formatted in .csv files. Data was then post-processed offline and entered to into the MATLAB software on a 1.80-GHz Intel Core i7 processor. Before further analysis of collected data, the noise produced from the function generator and driven by the optical transmitter was tested to determine if it followed the corresponding distribution. To verify that the additive white noise signal followed a Gaussian distribution, an empirical 1-D histogram was computed

for verification, shown in Figure 3-6. The histogram proved that the additive noise did indeed follow a Gaussian distribution, thus was fit for use in the research for this thesis.

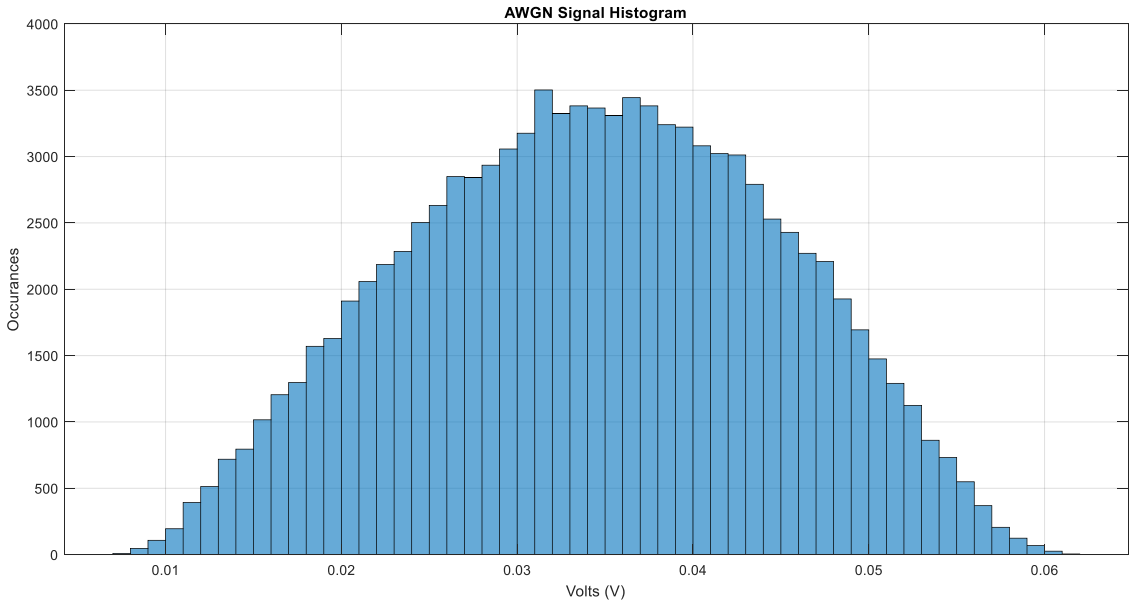

Figure 3-6. Additive noise empirical 1-D histogram.

The visual representation of three signals (i.e., 2000 samples for better visualization), along with their corresponding histograms (a) AWGN- (b) PRBS; and (c) combined signals are shown in Figures 3-7, -8, and -9, respectively.

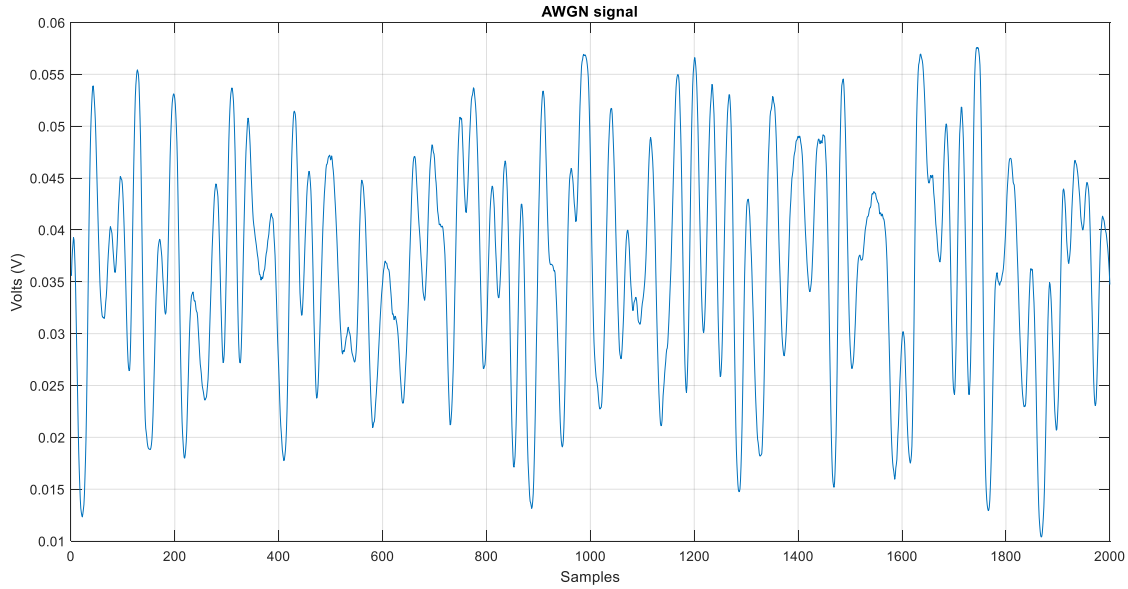

(a) Signal.

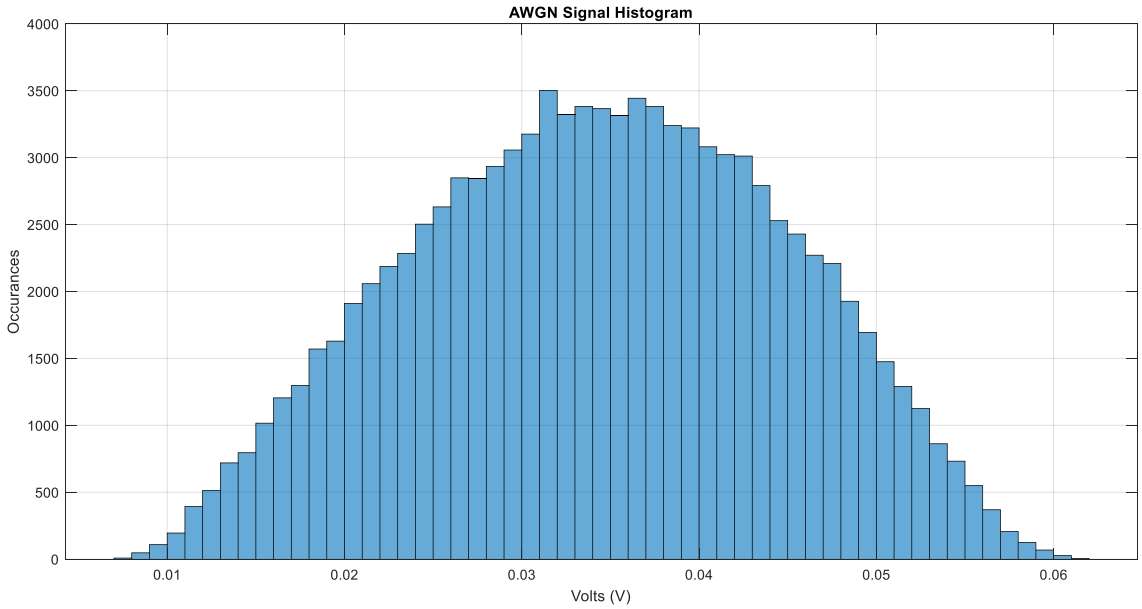

(b) Histogram.

Figure 3-7. Addition White Gaussian Noise (AWGN).

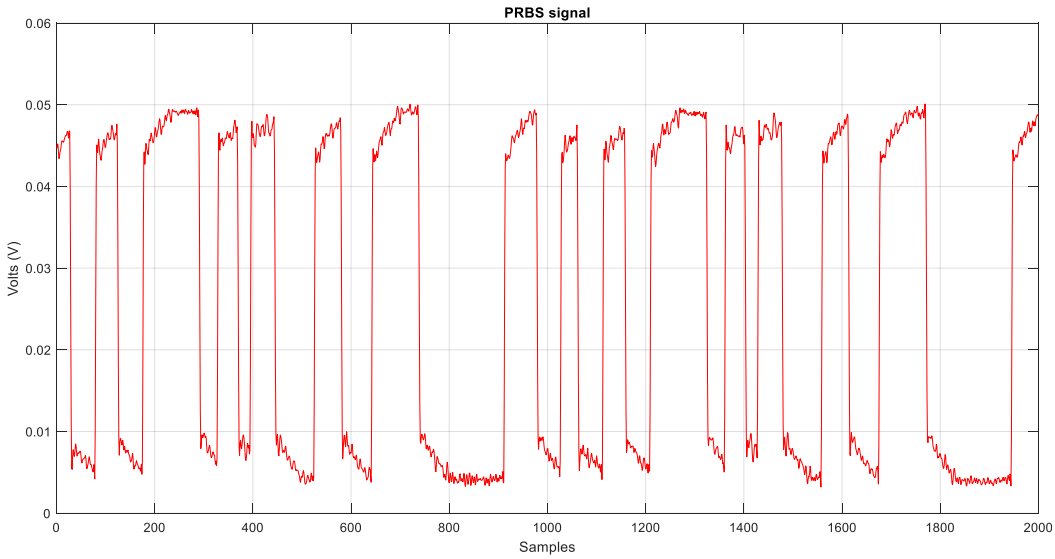

(a) Signal.

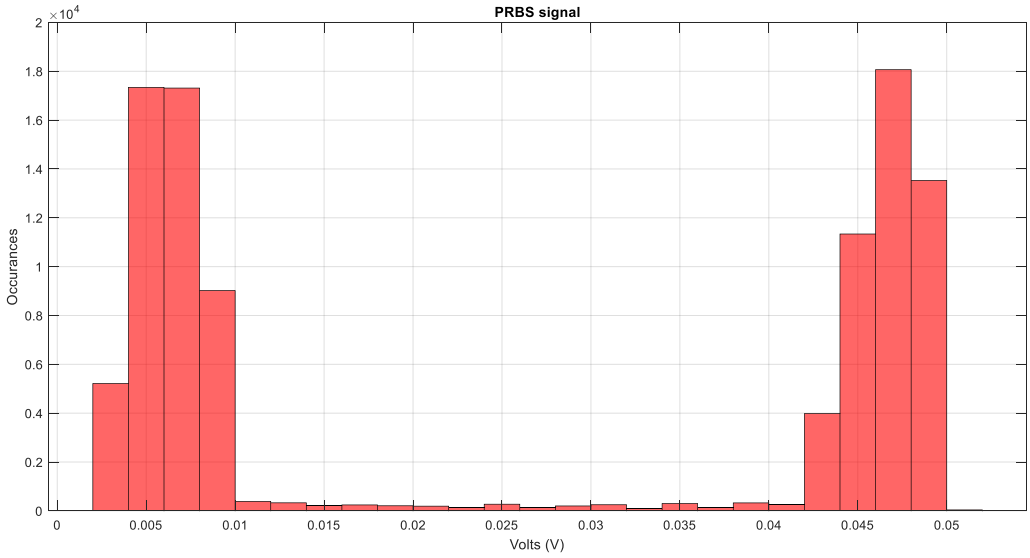

(b) Histogram.

Figure 3-8. Pseudorandom Binary Sequence (PRBS).

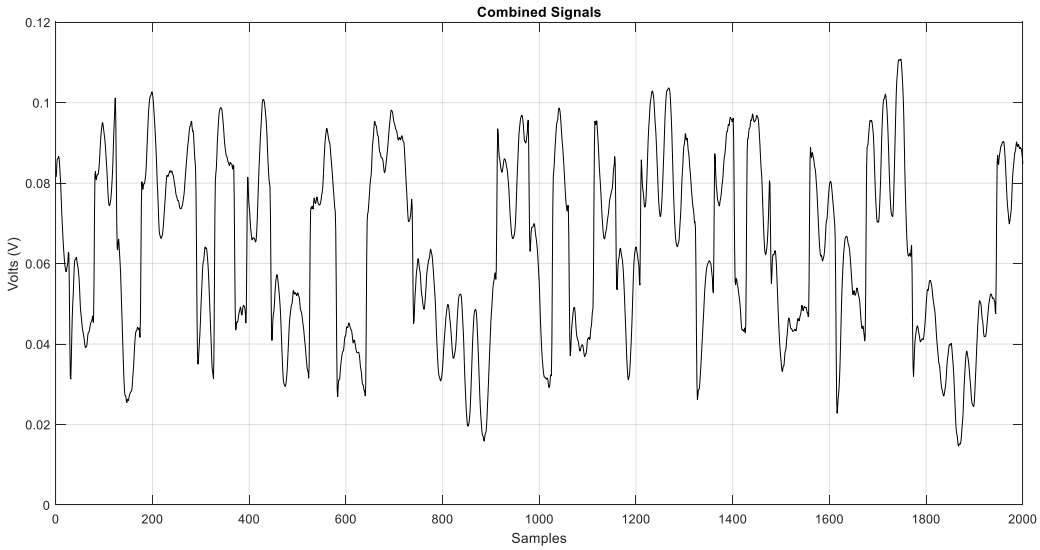

(a) Signal.

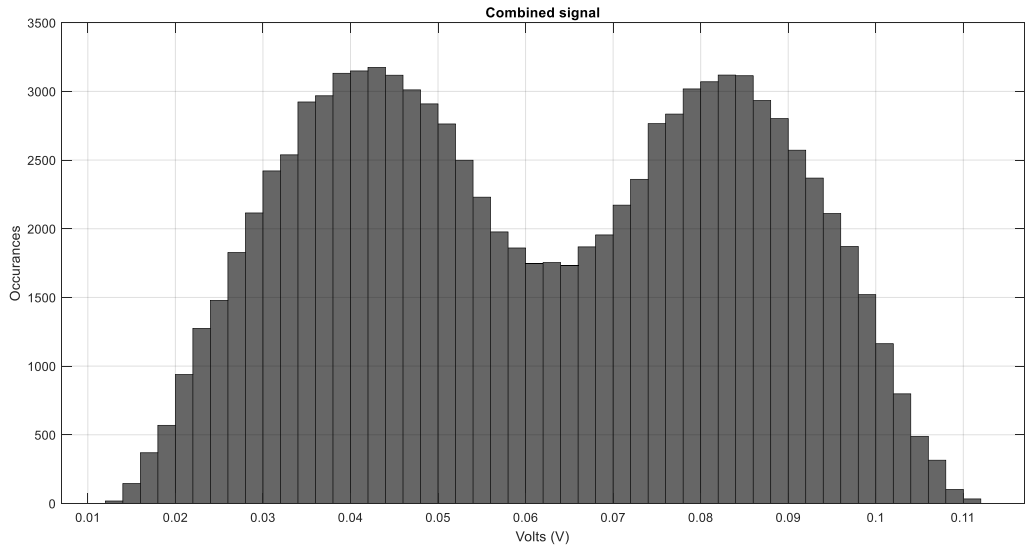

(b) Histogram.

Figure 3-9. Combined (PRBS + AWGN).

3.4 Results

3.4.1 Subtraction and Extraction of Synchronized Noise Signals

This section presents the subtraction method to used extract AWGN signals from the combined, noisy (PRBS + AWGN) signals. As mentioned in the previous section, 100,000 samples were collected for each of the three optical signals for this research. The acquired data was formatted in .csv files. Acquired data was entered into MATLAB in the form of 100,000x1 arrays. Because three signals were captured simultaneously, they were synchronized to the same time samples. Given the internal memory of the oscilloscope for data acquisition (i.e., 100,000 samples), normalized cross-correlation was used for evaluating performance of the extracted PRBS signal vs. the original PRBS signal. In Figure 3-10, the red and blue lines represent the combined signals and AWGN signals, respectively.

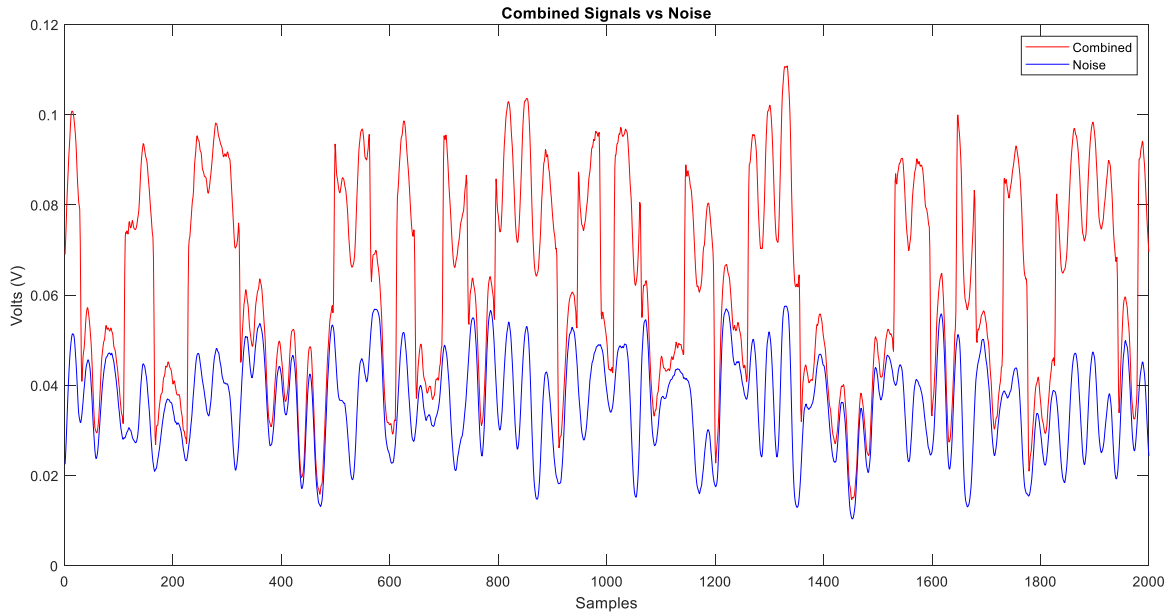

Figure 3-10. Synchronized combined (PRBS + AWGN) vs. AWGN signals.

Since channel state information (CSI) is known, extracted signals were reconstructed and subtracted from the combined, noisy received signal. Using the subtraction method, AWGN signal was shown and proven viable for subtraction from the combined signals for extracting the original PRBS signal. It was assumed that the ideal subtractor condition without loss signal occurs during subtraction. Figure 3-11 shows the original PRBS vs. extracted PRBS signal. Figure 3-12 shows that a normalized cross-correlation of 0.9964 was obtained for the PRBS signal vs. extracted PRBS signal.

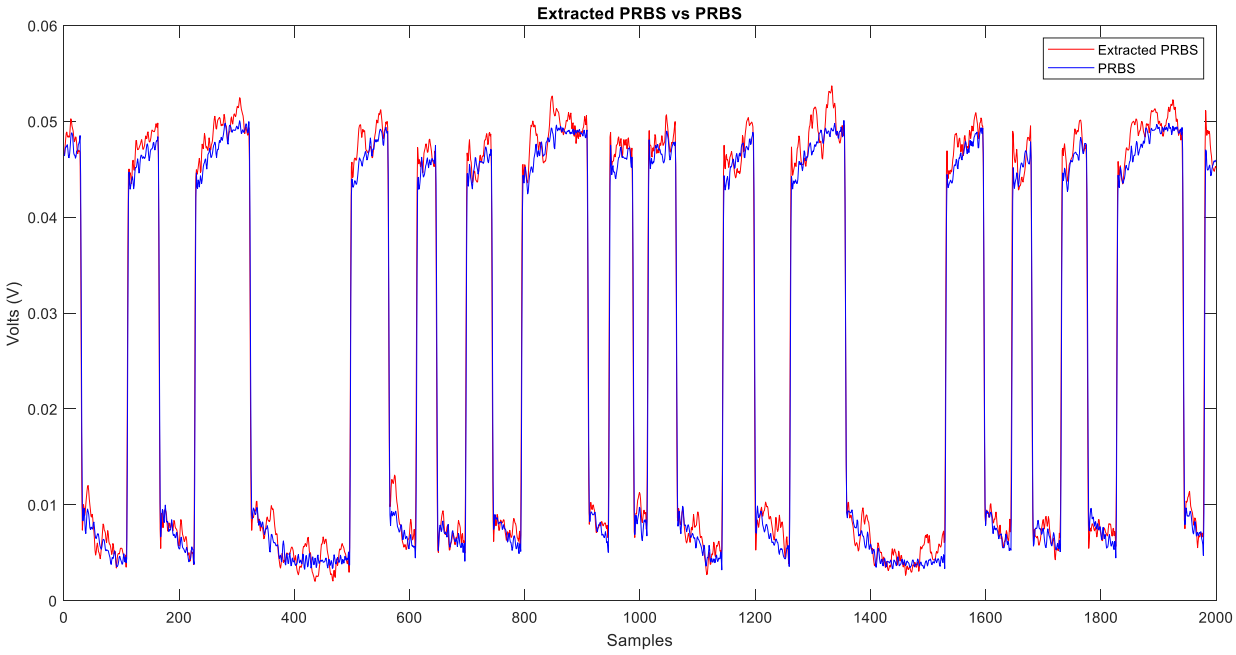

Figure 3-11. Original PRBS vs. extracted PRBS signal.

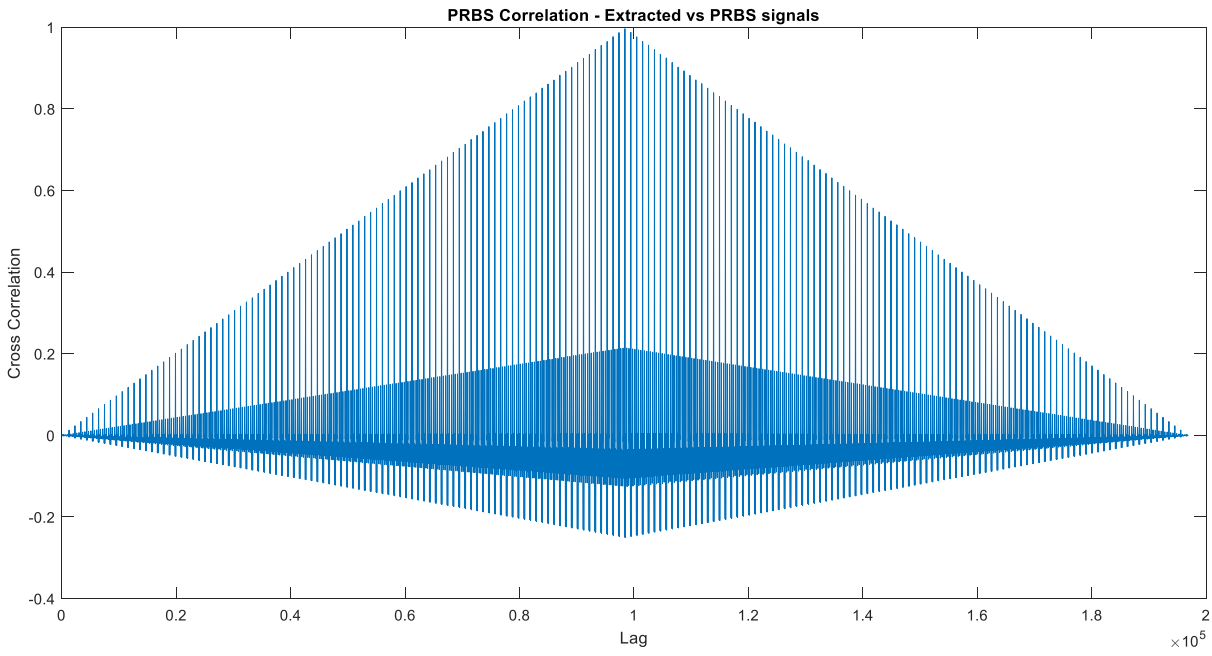

Figure 3-12. Normalized cross-correlation of PRBS vs. extracted PRBS signals.

Using this method demonstrates that the subtraction process can be used to extract the original PRBS signal from the combined, noisy signal when all three signals are simultaneously collected, at the receiver end and show nearly complete accuracy (i.e., cross-correlation of 0.9964).

3.4.2 Subtraction and Extraction of Unsynchronized Noise Signals

As mentioned above, the subtraction method of all three synchronized optical signals yields an accurate cross-correlation (i.e., 0.9964) of the original PRBS signal vs. the extracted PRBS signals.

To evaluate if the subtraction method can similarly be used to extract the PRBS signal from a combined, noisy signal, AWGN with the same parameters sigma (σ) and mu (μ), was used to subtract and analyze combined signal output.

Previously, the AWGN signal was simultaneously captured with the same sample sequence as the original PRBS and Combined signals. In this analysis, when using the same subtraction method, the random AWGN signal (i.e., blue lines) with known sigma (σ) and mu (μ) parameters—albeit collected on its own with separate time sample, was subtracted from the combined, noisy signal (i.e., red lines), as shown in Figure 3-13.

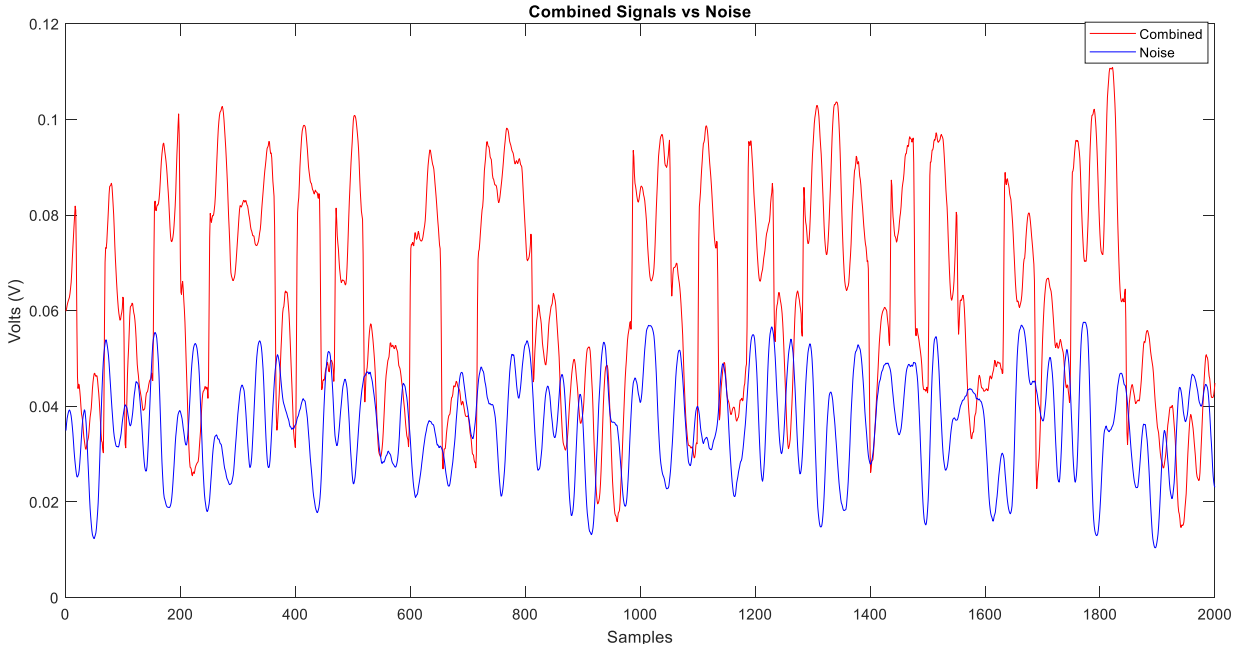

Figure 3-13. Unsynchronized combined (PRBS + AWGN) vs. AWGN signals.

Figure 3-14 displays the original PRBS vs. extracted PRBS signal. Additionally, Figure 3-15 shows that a normalized cross-correlation of 0.8044 was obtained for the PRBS signal vs. extracted PRBS signal, when a random, unsynchronized AWGN signal with known parameters was subtracted from the combined, noisy signal.

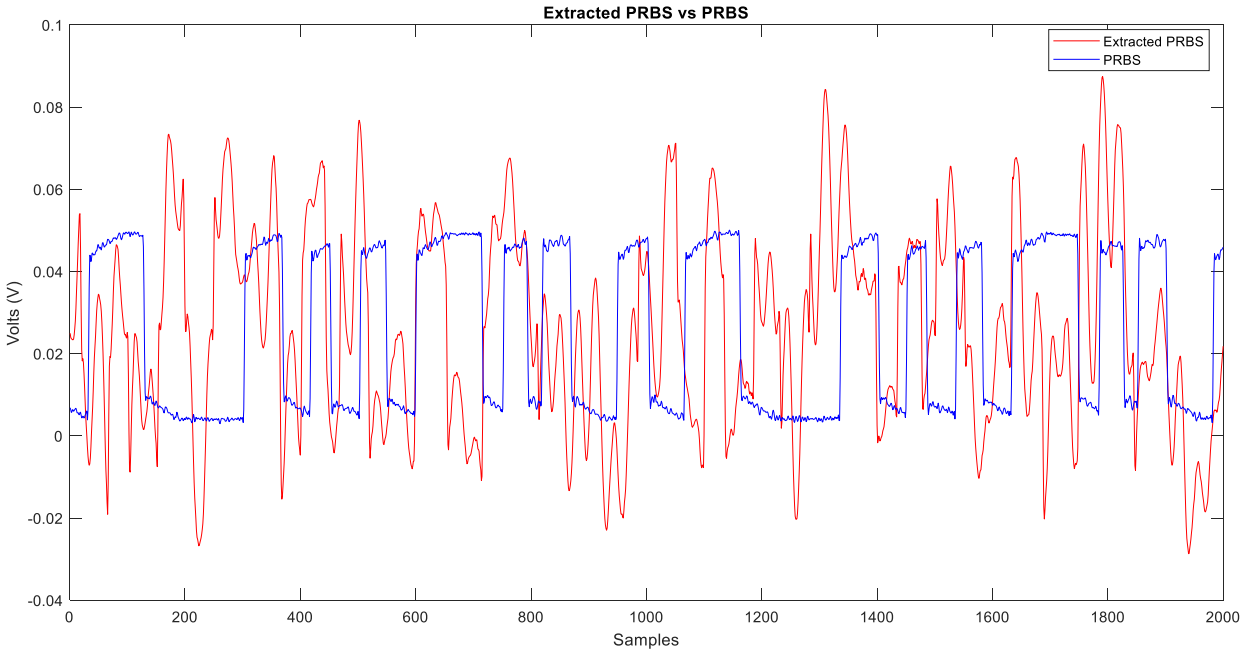

Figure 3-14. Original PRBS vs. extracted PRBS signals.

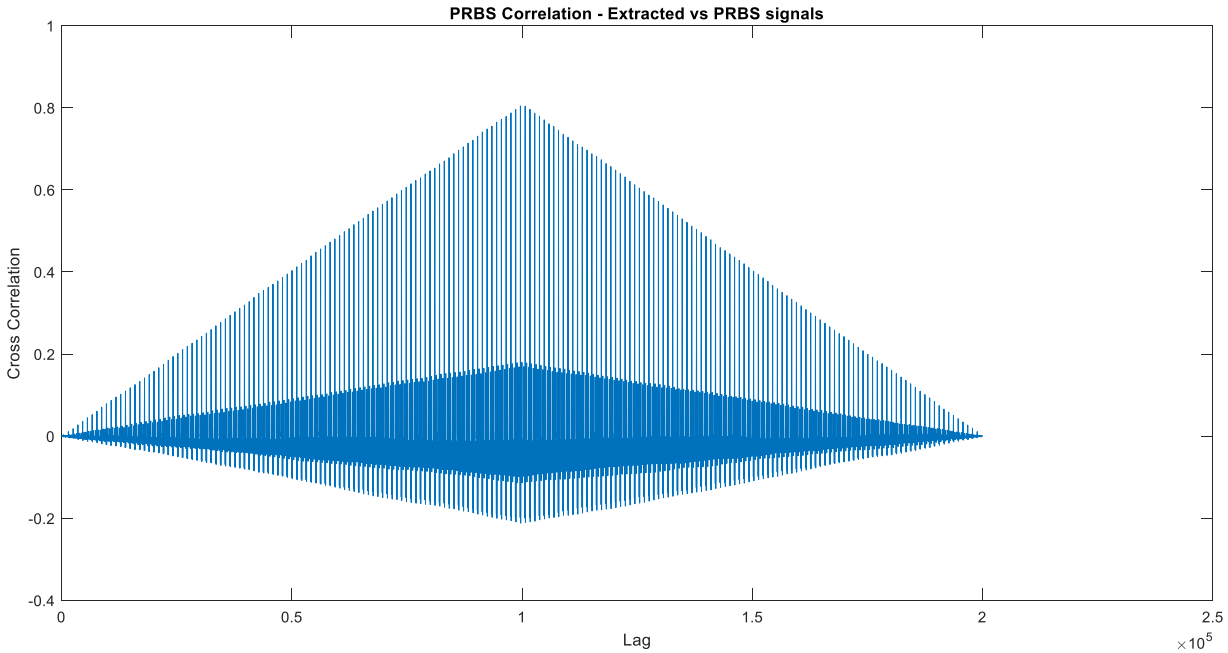

Figure 3-15. Normalized cross-correlation of PRBS vs. extracted PRBS signals.

3.4.3 Signal-to-Noise Ratio (SNR)

To quantify the performance of a direct detection receiver, the output signal-to-noise ratio (SNR) is defined as the ratio of the detector signal power to the total noise power. In practice, the received power is typically large enough such that the signal current dominates over the dark current and background illumination noise

SNR serves as a benchmark indicator for optical transmission system performance assessment. SNR values most valued are at the receiver end. Consequently, a low SNR indicates that the receiver will most likely not detect or recover the signal as well as a higher SNR value. The SNR limit is one of the key parameters that determine how far a wavelength can travel prior to regeneration.

The optical SNR ratio is given by the equation,

$$\text{SNR} = 10\ \text{dB} \cdot \log_{10}\left(\frac{Signal}{Noise}\right) \qquad \text{Eq. (2)}$$

The signal given in Eq. (1) is represented by the range of the original PRBS signal, which is the difference between the maximum and minimum values of the input data signal itself. On the other hand, the noise in Eq. (1) is represented by the range of the AWGN, which remained constant during the SNR calculation, only varying PRBS signal range.

SNR was utilized to observe cross-correlation accuracy of the original PRBS vs. extracted PRBS signals vs. SNR (dB), as shown in Figure 3-16. Results demonstrated that cross-correlation of the extracted PRBS signal vs. the original PRBS signal increased as SNR increased, meaning that as PRBS signal power—compared to AWGN power,—increased, the extracted PRBS signal vs. original PRBS cross-correlation increased. In other words, the extracted PRBS signal was more fitting to extract when the PRBS signal power dominated the AWGN signal power.

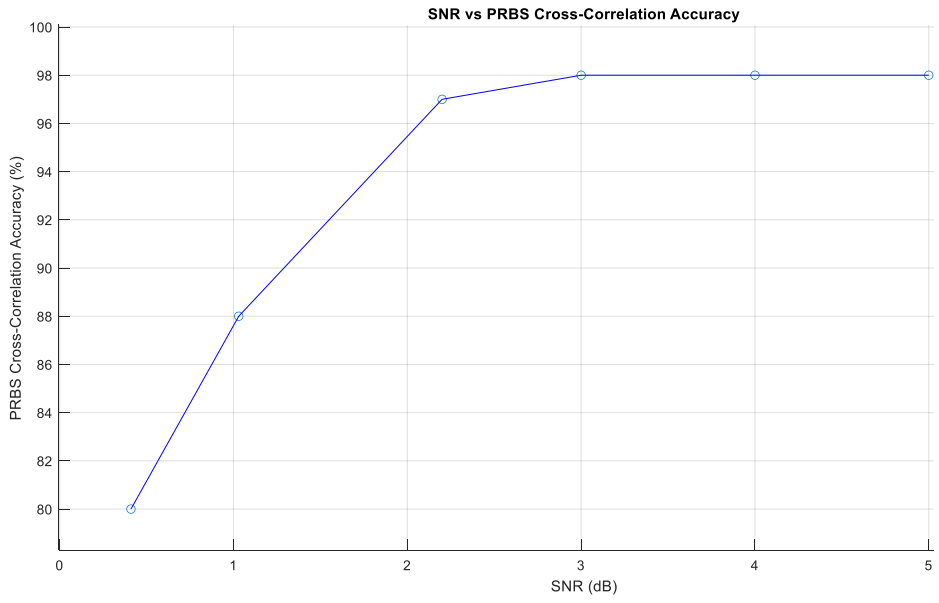

Figure 3-16. SNR vs. PRBS cross-correlation accuracy.

3.4.4 Jitter

Jitter is the random delay occurring from the time a photon is incident on a photo-detector to the time a photoelectron is detected. Figures in the previous section evidenced that, PRBS, AWGN, and combined signals were simultaneously collected in the same time sample sequences. Consequently, the subtraction process was leveraged to extract the PRBS signal, compared to the original PRBS signal with almost ideal cross-correlation (i.e., 0.9964). In this scenario it was assumed that there was no jitter in collected signals.

To further investigate the effects on these signals, the AWGN signal was jittered before it was subtracted from the combined, noisy signal. Figure 3-17 shows that as the jitter increased, cross-correlation accuracy between the extracted PRBS signal vs. the original PRBS signal decreased. This proposes that as the AWGN signal becomes no longer synchronized with the combined, noisy signal, the accuracy of PRBS decreases. At and around 20 jitter samples (i.e., 20 ns), cross-correlation hovers at approximately 75- to 77% cross-correlation (i.e., 0.75-0.77) accuracy, implying that the PRBS signal reassembles over the extracted PRBS signal throughout all time samples collected.

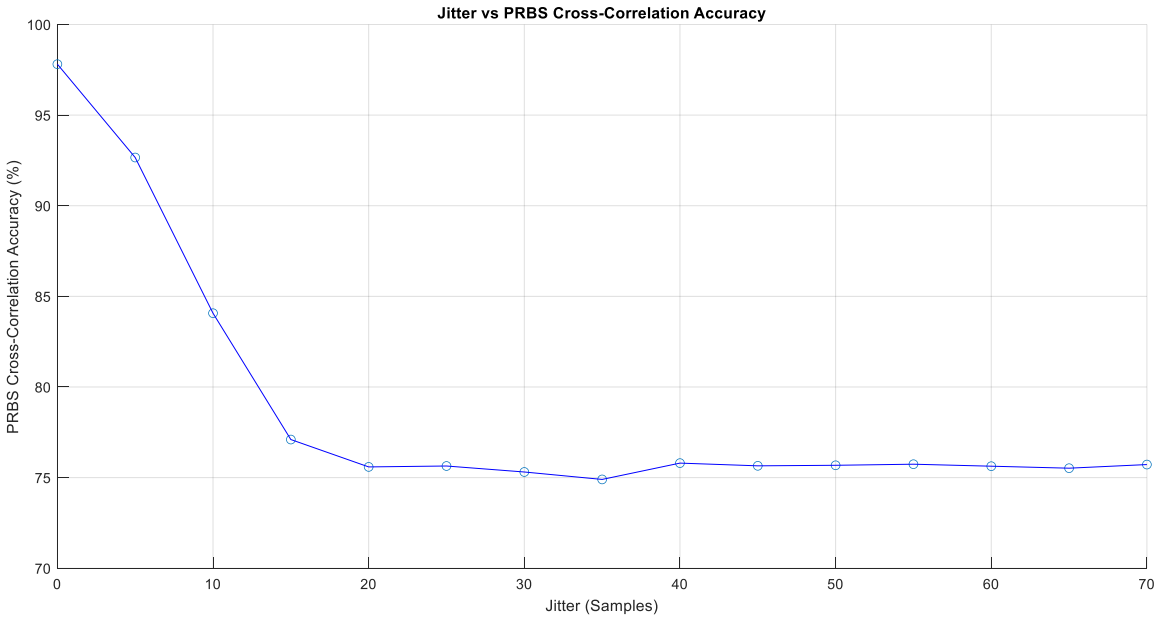

Figure 3-17. Jitter vs. PRBS cross-correlation accuracy.

Chapter 4: GAUSSIAN MIXTURE MODEL (GMM)

4.1 Motivation

As demonstrated and proven in the previous sections, the subtraction method was successfully used to extract AWGN signals from the combined, noisy signals when the AWGN parameters were previously known. The motivation behind choosing GMM was finding a model to derive, output, and estimate the AWGN parameters sigma (σ) and mu (μ) in order to generate a random AWGN signal with the estimated parameters for subtracting and extracting the AWGN from the combined, noisy signal (e.g., PRBS + Noise) in this thesis research work. In addition, GMMs maintain many of the theoretical and computational benefits of Gaussian models, making them practical for efficiently modeling large datasets. Recall that in Figure 3-8(b), the histogram of the combined, noisy signal has two peaks, which suggests that data might follow a mixture model.

4.2 The Model

A GMM is a parametric probability density function represented as a weighted sum of Gaussian component densities. GMMs are commonly used as a parametric model of the probability distribution of continuous measurements or features in an application system. GMM parameters are estimated from training data using the iterative expectation-maximization (EM) algorithm or maximum a posteriori (MAP) estimation from a prior signal (i.e., combined, noisy signal) in this model.

A GMM is a weighted sum of M component Gaussian densities, as given by the equation,

$$p(x|\lambda) = \sum_{i=0}^{M} \omega_i g(x|\mu_i, \Sigma_i) \qquad \text{Eq. (3)}$$

where x D-dimensional continuous-valued data vector (i.e. measurement or features), ω_i, $i = 1, \ldots, M$, are the mixture weights, and $g(x|\mu_i, \Sigma_i), i = 1, \ldots, M$ are the component Gaussian densities. Each component density is a D-variate Gaussian function of the form,

$$g(x|\mu_i, \Sigma_i) = \frac{1}{(2\pi)^{\frac{D}{2}}|\Sigma_i|^{\frac{1}{2}}} \exp\{-\frac{1}{2}(x - \mu_i)' \sum_i^{-1}(x - \mu_i)\}, \qquad \text{Eq. (4)}$$

with mean vector μ_i and covariance matrix Σ_i. The Mixture weights satisfy the constraint that $\sum_{i=1}^{M} \omega_i = 1$. The complete GMM is parameterized by the mean vectors, covariance matrices and mixture weights from all component densities. Parameters are collectively represented by the notation,

$$\lambda = \{\omega_i, \mu_i, \Sigma_i\} \qquad i = 1, \ldots, M. \qquad \text{Eq. (5)}$$

Several variants of GMM shown in Equation (3). Covariance matrices, Σ_i, can be full rank or constrained to be diagonal. Additionally, parameters can be shared or tied among Gaussian components (e.g., having a common covariance matrix for all components). Model configuration selection (i.e., number of components, full or diagonal covariance matrices, and parameter tying) is often determined by the amount of data available for estimating GMM parameters and how GMM is used in a particular application. The number of components and distributions used in this research work is discussed below.

4.3 Data Estimation

The research reported herein proposes using MATLAB's GMM functions to estimate the AWGN parameters, and then generate a random AWGN signal using the estimated parameters for extracting the additive noise from the combined, noisy signals. The GMMs require that the component number is specified before being fit to data, which aids in estimating parameters.

MATLAB's `fitgmdist (X, k)` function returns a Gaussian mixture distribution model (GMModel) with k components fitted to data (X) with X being the combined, noisy signals (PRBS + AWGN); and k being the number of components used. The `fitgmdist (X, k)` function was used, as shown in Figure 4-1.

For many applications it might be difficult to determine the appropriate number of components. Thus, the empirical 1-D histogram for combined signals (PRBS + AWGN) was computed, as demonstrated in Figure 4-1. Number of detected distributions was provided as input for the number of components to use when fitting the signal into the GMM. Figure 4-1 shows that the number of detected peaks in the 1-D histogram function was 2. Hence, 2 was used as input for the number of distributions for the GMM. Additionally, Figure 4-2 displays all three histograms for PRBS (See blue histogram), AWGN (See coral histogram), and combined, noisy signals (See orange histogram).

```
gm = fitgmdist(X, k);

gm = fitgmdist(CombinedSignal, 2);
```

Figure 4-1. MATLAB's Gaussian Mixture Model fitted to data.

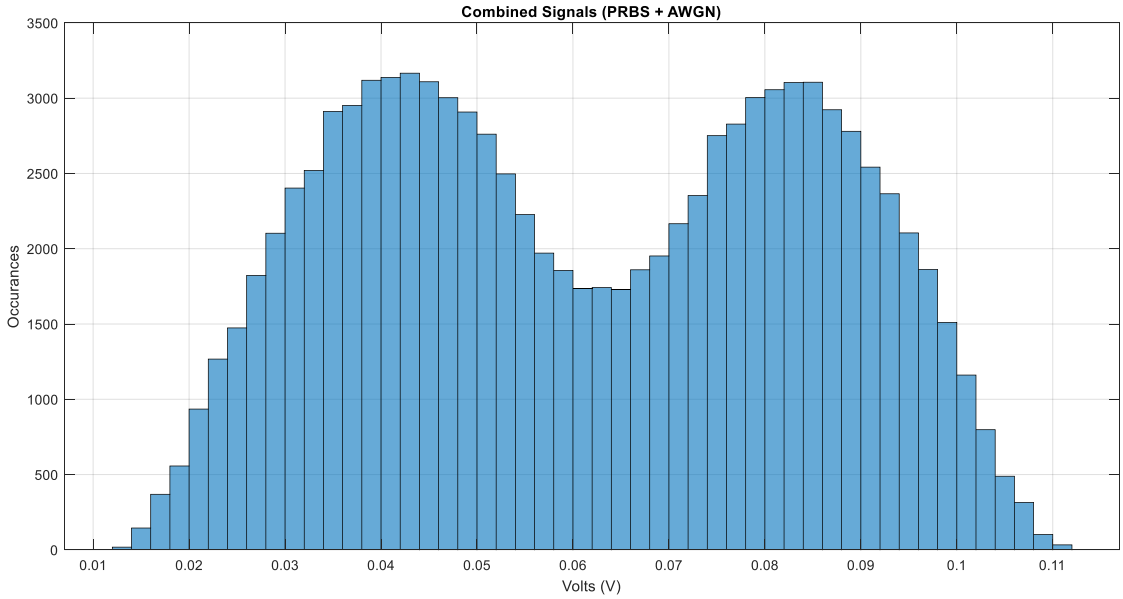

Figure 4-2. Combined (PRBS + AWGN) signals empirical 1-D histogram.

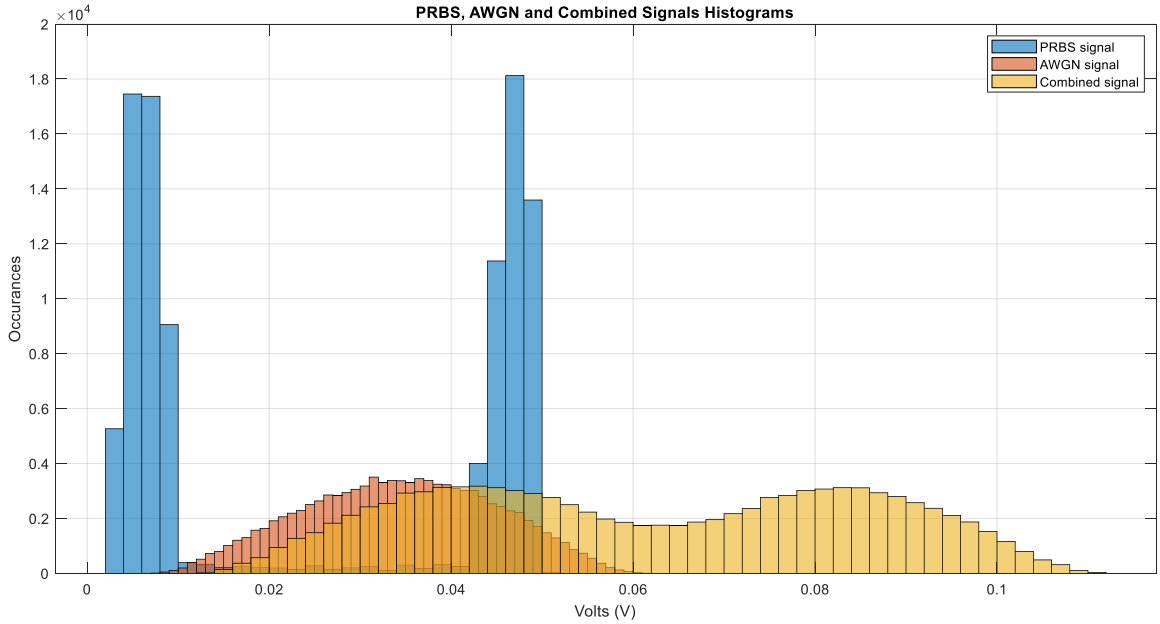

Figure 4-3. PRBS, AWGN and combined (PRBS + AWGN) signals empirical 1-D histogram.

4.4 Results

The effectiveness and estimated output parameters from the GMM, random AWGN signal generation, subtraction method, and analysis are reported in this section.

The MATLAB software system fitted GMM with two distinct means, covariances matrices, and component proportions to the data (i.e., combined, noisy signals). A depiction of the GMM is simplified in Figure 4-3.

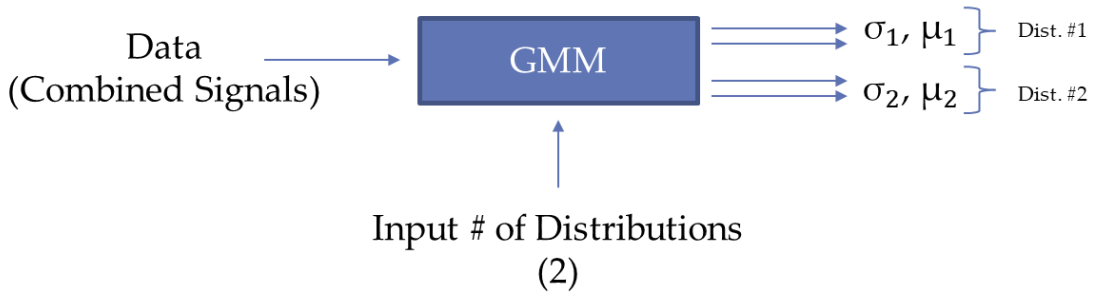

Figure 4-4. Simplified depiction of the Gaussian Mixture Model.

The GMM outputs two distributions with separate estimates for parameters, (σ_1, μ_1) and (σ_2, μ_2), respectively. GMM output in illustrated in Figure 4-4 below.

```
>> gm

gm =

Gaussian mixture distribution with 2 components in 1 dimensions

Component 1:

Mixing proportion: 0.472597

Mean:    0.0829


Component 2:

Mixing proportion: 0.527403

Mean:    0.0426


>> gm.Sigma

ans(:,:,1) =

   0.012659


ans(:,:,2) =

   0.014836
```

Figure 4-5. MATLAB's Gaussian Mixture Model output.

Based the histograms shown in Figure 4-2, one can see that the component with the smaller mean (mu, μ) (i.e., component 2) corresponds to the AWGN estimated parameter output. Table 4.1 displays the parameters, standard deviation (sigma, σ) and mean (mu, μ) of the known and estimated AWGN generated from the GMM.

Table 4.1. Comparison of Known and Estimated AWGN parameters

Additive White Gaussian Noise	Standard Deviation (σ)	Mean (μ)
Original AWGN	0.0139	0.0459
Estimated AWGN	0.0148	0.0426

Next, using estimated parameters—sigma (σ) and mu (μ), an AWGN signal was generated using MATLAB's `normrnd(mu,sigma)` function. Figure 4-5 shows how the function generates a random number from the normal distribution with mean parameter, mu, and standard deviation parameter, sigma, given from the GMM output. In addition to sigma and mu parameters, '100,000' and '1' represent the number of samples needed to generate a 100,000x1 array, as per the collected signals described in previous sections of this thesis.

```
RandomAWGN = normrnd(μ, σ, 100000, 1);

RandomAWGN = normrnd(0.0426, 0.0148, 100000, 1);
```

Figure 4-6. MATLAB's function used for AWGN signal generation.

Figure 4-6 shows an empirical 1-D histogram to verify that the random AWGN signal generated on MATLAB follows the AWGN parameters and distribution and offers a comparison with the original AWGN signal collected from the oscilloscope.

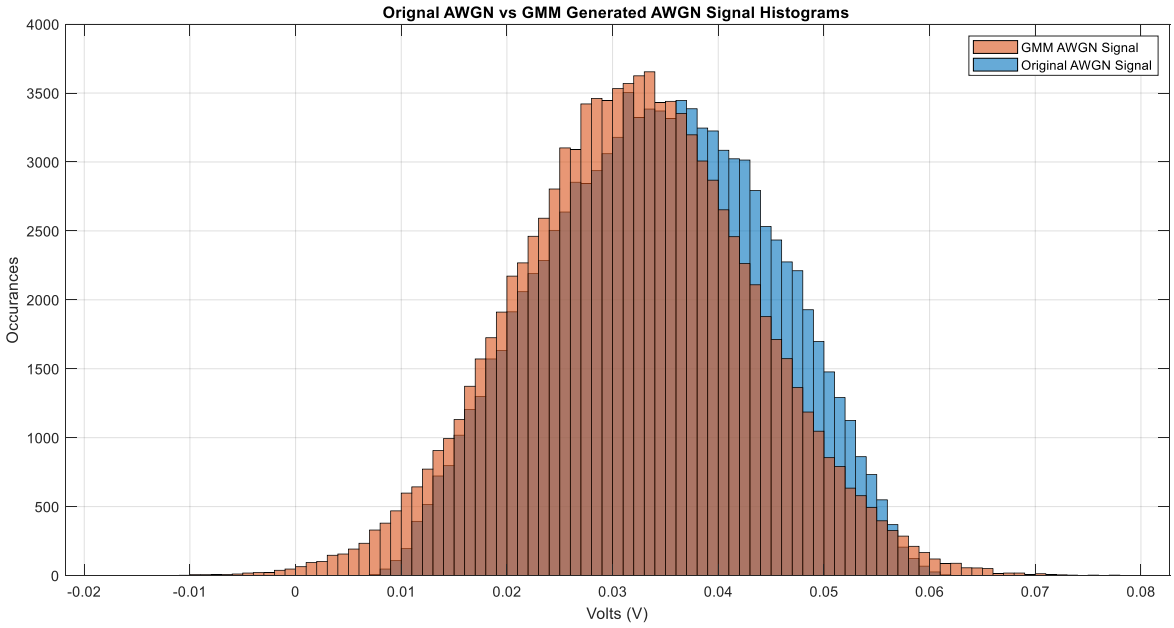

Figure 4-7. Original vs. GMM-estimated AWGN signal empirical 1-D histograms

The orange histogram represents the AWGN signal generated from the estimated GMM parameters; the blue histogram represents the original AWGN signal with known parameters.

Furthermore, using the subtraction method as detailed in the previous sections, the newly estimated and generated AWGN signal is subtracted from the combined, noisy signal. Normalized cross-correlation was utilized for evaluating performance of the extracted PRBS signal vs. the original PRBS signal. Results in Figure 4-7 show that a normalized cross-correlation of 0.7952 was obtained for the PRBS signal vs. extracted

PRBS signal, when an AWGN signal with estimated parameters from the GMM, was subtracted from the combined, noisy signal.

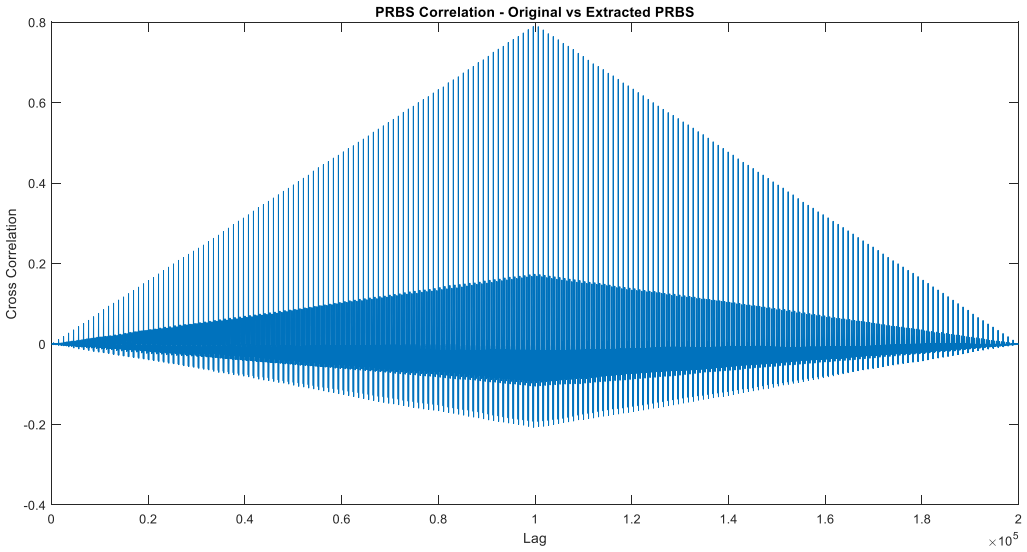

Figure 4-8. Normalized cross-correlation of PRBS vs. extracted PRBS signals

CHAPTER 5: CONCLUSION AND FUTURE WORK

5.1 Conclusion

The new, high data-rate and high bandwidth services/applications required by the forthcoming terrestrial, aerial, and space networks dramatically increase the demand for wireless capacity. FSOC has been considered a promising technology for meeting these needs and supporting high data-rate, high capacity, low power consumption, secure, and high-density networks. Such requirements mean that next-generation wireless networks will face increased system complexity, especially due to the heterogeneity of supported services, applications, devices, and transmission technologies.

Background noise is a significant problem for FSOC, even when there are no weather and/or atmospheric turbulences. In fact, signal transmission is significantly affected by background noise, mostly at the receiver end. An additive AWGN channel is assumed, wherein background illumination is the dominant source of noise.

The research work highlighted in this thesis achieved three key objectives: a) to gain increased understanding of FSOC; b) learn more about the effects of background noise affecting and deteriorating signals; and c) conducting the experimental setup and analysis for extracting AWGN from an affected signal with background noise through the use of the subtraction method. These objectives were investigated and experimentally validated to separate/subtract and extract additive noise signals from a combined, noisy signal.

The subtraction method was confirmed to achieve these promising results. Tests and data analysis were conducted for one PRBS user affected with known AWGN parameters, while synchronized without time delays. After subtracting AWGN from the combined, noisy signal, a normalized cross-correlation between the original PRBS and

extracted PRBS—greater than 0.99—was accomplished. Furthermore, a random AWGN signal with known parameters was extracted from the combined, noisy signal to show a normalized cross-correlation between the original PRBS and extracted PRBS of about 0.80. Lastly, GMM was used, and its results proved successful estimation of AWGN parameters, namely sigma and mu, for extracting the noise from a combined, noisy signal when the initial AWGN parameters were unknown.

5.2 Future Work

Work presented in this thesis confirms that FSOC technology is a promising endeavor. Successful completion of investigations reported herein lays the groundwork for future work. Several hardware, software, and testing research efforts could be pursued for practical realization of an FSOC system. Accordingly, this thesis concludes by posing the following research questions that should direct future research.

- This work examined one user combined with an AWGN signal. Is it possible to combine at least two users with different PRBS parameters and AWGN, and then use the subtraction method to extract the noise?
- Is it possible to emulate and apply the subtraction method to extract noise from a combined signal with a different additive noise signal?
- What other communication/performance parameters could be estimated to facilitate and separate signals from additive background noise?
- What effects does the modulation have on the combined, noisy signal? Can two users transmitting have different modulations?

REFERENCES

[1] "Free Space Optics (FSO) and Visible Light Communication (VLC)/Light Fidelity (Li-Fi) Market Insights, Trends | Industry Report, 2025 | MarketsandMarkets™." https://www.marketsandmarkets.com/ResearchInsight/visible-light-communication-market.asp

[2] V. Jain, H. Kaushal, and A. Vats, "Free space optical communication: laser sources, modulation schemes and detection techniques," *Int. Conf. Telecommunication Netw.*, no. March 2018, 2013

[3] H. Kaushal and G. Kaddoum, "Optical Communication in Space: Challenges and Mitigation Techniques," *IEEE Communications Surveys and Tutorials*, vol. 19, no. 1. Institute of Electrical and Electronics Engineers Inc., pp. 57–96, Jan. 01, 2017

[4] I. I. Smolyaninov, L. Wasiczko, K. Cho, and C. C. Davis, "Long-distance 1.2 Gb/s optical wireless communication link at 1550 nm," *Free. Laser Commun. Laser Imaging*, vol. 4489, no. June 2014, pp. 241–250, 2002, doi: 10.1117/12.453237.

[5] "Optical Wireless Communications: System and Channel Modelling with MATLAB®, Second Edition

6] E A Park, D Cornwell, and D Israel. NASA's Next Generation ≥100 Gbps Optical Communications Relay. In 2019 IEEE Aerospace Conference, pages 1–9, 2019

[7] "Deep Space Optical Communications (DSOC)," *NASA*. https://gameon.nasa.gov/archived-projects-2/deep-space-optical-communications-dsoc/.

[8] fSONA unveils 2-5-Gbps free-space optical systems. September 5, 2012.

[9] Xiaoming Zhu and J. M. Kahn, "Free-space optical communication through atmospheric turbulence channels," in IEEE Transactions on Communications, vol. 50, no. 8, pp. 1293-1300, Aug. 2002, doi: 10.1109/TCOMM.2002.800829.

[10] J. Katz, "Planets as background noise sources in free space optical communication," Adv. Electron. Mater. Devices Section, TDA Progr. Rep. 42-85, 1986.

[11] Kwonhue Choi; Huaping Liu, "Maximum Likelihood Detection for Binary Transmission," in Problem-Based Learning in Communication Systems Using MATLAB and Simulink , IEEE, 2016, pp.174-183, doi: 10.1002/9781119060239.ch16.

[12] E.A. Lee, D.G. Messerschmitt, Digital Communication, (Kluwer Academic Publishers, Boston, 1994)

[13] Hemani Kaushal, V K Jain, and Subrat Kar. Free Space Optical Communication. Springer, 2017

[14] S. M. Navidpour, M. Uysal, and M. Kavehrad, "BER performance of free-space optical transmission with spatial diversity," IEEE Trans. Wireless Commun., vol. 6, pp. 2813–2819, Aug. 2007

[15] T. A. Tsiftsis, H. G. Sandalidis, G. K. Karagiannidis, and M. Uysal, "Optical wireless links with spatial diversity over strong atmospheric turbulence channels," IEEE Trans. Wireless Commun., vol. 8, pp. 951– 957, Feb. 2009.

[16] X. Zhu and J. M. Kahn, "Free-space optical communication through atmospheric turbulence channels," IEEE Trans. Commun., vol. 50, pp. 1293–1300, Aug. 2002.

[17] S. Arnon, "Optimization of urban optical wireless communication systems," IEEE Trans. Wireless Commun., vol. 2, pp. 626–629, July 2003.

[18] M. Uysal, S. M. Navidpour, and J. Li, "Error rate performance of coded free-space optical links over strong turbulence channels," IEEE Commun. Lett., vol. 8, pp. 635–637, Oct. 2004.

[19] W. Gappmair, S. Hranilovic, and E. Leitgeb, "Ook performance for terrestrial fso links in turbulent atmosphere with pointing errors modeled by hoyt distributions," IEEE Commun. Lett., vol. 15, pp. 875–877, Aug. 2011.

[20] S. Rajbhandari, Z. Ghassemlooy, P. A. Haigh, T. Kanesan, and X. Tang, "Experimental error performance of modulation schemes under a controlled laboratory turbulence fso channel," IEEE/OSA J. Lightwave Technol., vol. 33, pp. 244–250, Jan. 2015

[21] W. Gappmair, "Further results on the capacity of free-space optical channels in turbulent atmosphere," IET Communications, vol. 5, pp. 1262–1267, June 2011.

[22] C. C. Chen and C. S. Gardner, "Impact of random pointing and tracking errors on the design of coherent and incoherent optical intersatellite communication links," IEEE Trans. Commun., vol. 37, pp. 252–260, Mar. 1989

[23] D. K. Borah, D. Voelz, and S. Basu, "Maximum-likelihood estimation of a laser system pointing parameters by use of return photon counts," Appl. Opt., vol. 45, pp. 2504–2509, Apr. 2006.

[24] D. K. Borah and D. G. Voelz, "Pointing error effects on free-space optical communication links in the presence of atmospheric turbulence," J. Lightw. Technol., vol. 27, no. 18, pp. 3965-3973, Sep. 2009.

[25] F. Aveta, H. H. Refai and P. LoPresti, "Multi-user detection in optical wireless communication," *2019 15th International Wireless Communications & Mobile Computing Conference (IWCMC)*, Tangier, Morocco, 2019, pp. 214-219